Excitation and detection of surface acoustic phonon modes in Au/Al_2O_3 multilayers

A. Halabica, S. T. Pantelides,* and R. F. Haglund, Jr.
Department of Physics and Astronomy, Vanderbilt University, 6301 Stevenson Center, Nashville, Tennessee 37235, USA

R. H. Magruder III
Department of Chemistry and Physics, Belmont University, 1900 Belmont Boulevard, Nashville, Tennessee 37212, USA

A. Meldrum
Department of Physics, University of Alberta, Edmonton, Alberta, Canada T6G 2J1
(Received 24 July 2009; published 22 October 2009)

A time-resolved pump-probe technique was used to observe the surface acoustic modes of Au/Al_2O_3 multilayers. As the thickness of the Au layers was increased from 2 to 5 nm, a change in the excitability of particular surface phonon modes with frequencies up to 200 GHz was observed. We compare our results with transfer-matrix theoretical calculations. In addition, we model the superlattice in a finite element simulation environment and use the data to evaluate the excitability of the surface modes. The model predictions correlate well with the experimental data. Simultaneous excitation of the surface and normal (propagating) phonon modes is observed in the Au(5 nm)/Al_2O_3(45 nm) superlattice. The normal modes allow us to calculate the effective sound velocity of the superlattice, which agrees well with the theory calculation.

DOI: 10.1103/PhysRevB.80.165422 PACS number(s): 63.22.Np, 68.65.Cd, 78.47.J−, 78.67.Pt

I. INTRODUCTION

Ultrafast time-resolved techniques have been successfully used to study the coherent acoustic vibrations of nanometer-scaled multilayers and superlattices of various compositions.[1–6] The periodicity of these structures causes folding of the phonon dispersion curve which gives rise to minibranches, separated by gaps at the zone boundaries. The band gaps are a direct consequence of the difference in elastic properties of the constituent layers and represent a frequency region in which no propagating phonon modes exist. However, theory predicts that localized surface modes can exist in the gaps when the superlattice is semi-infinite.[7,8]

In metallic superlattices,[6] softening of the longitudinal elastic constant with decreasing thickness $d_{1,2}$ of the constituent layers was observed. A similar effect was observed also in a metal/dielectric superlattice.[3] This elastic anomaly is generally ascribed to interfacial effects. The relative thickness ratio $\Gamma(=d_{1,2}/d; d=d_1+d_2)$ in most of the previous multilayer studies is in the range 0.3 to 0.7. By contrast, in the present work, we are studying metal/dielectric superlattices with the relative metal thickness ratio $\Gamma(=d_M/d) \leq 0.1$. It is interesting to study how the varying metal layer thickness influences the overall elastic properties of these dielectric dominated multilayers.

In this paper we report on the properties of the surface modes of Au/Al_2O_3 superlattices using time-resolved spectrocopy. The excitability and detectability of the surface modes are studied as a function of the thickness of Au layers. As the Au layer thickness is increased from 2 to 5 nm, the first band-gap surface mode becomes dominant and clearly detectable, while the second band-gap surface mode is observed in all samples. The experimental results are compared to theoretical calculations[4] combined with finite element modeling of the multilayer structure. In addition to the surface modes, the excitation of normal modes is observed in the Au(5 nm)/Al_2O_3(45 nm) superlattice.

II. EXPERIMENT

A time-resolved pump-probe technique was used to measure the photo-induced reflectivity change in superlattices.[9] Optical absorption of the ultrashort pump pulse sets up a thermal stress that impulsively excites strain waves in the multilayer structure. These waves generate a change in reflectivity via the photoelastic effect, which is observed with a time-delayed probe pulse. Optical pulses of a mode-locked Ti:sapphire laser (Mira 900) at 830 nm were used in our experiments. The full width at half maximum pulse duration is 120 fs and the repetition rate is 76 MHz. The pump beam is modulated by an acousto-optic (AO) modulator at a frequency of 53 kHz for lock-in detection. Pump and probe beams are both focused using the same lens onto a spot having a diameter of roughly 100 μm. The pump beam is at normal incidence to the sample surface, while the angle of incidence of the probe beam is less then 10°.

The multilayer films were deposited on fused silica substrates kept at room temperature. The Al_2O_3 layers were deposited using electron beam evaporation and the Au layers using thermal evaporation from a tungsten boat. Since both of these evaporation techniques were available in our deposition system, the samples were inside the vacuum chamber during the entire deposition process. The vacuum prior to deposition was 10^{-7} Torr. The superlattices all start and also terminate with an Al_2O_3 layer. The thickness of all Al_2O_3 layers was 45 nm, while the thickness of Au layers was varied from 2 to 5 nm. The number of periods is 10. Transmission electron microscopy (TEM) was used to analyze the structure of Au layers in a Au(2 nm)/Al_2O_3(20 nm) sample with 8 periods. In order to determine the elastic properties of the amorphous Al_2O_3 layers, two samples of a single Al_2O_3 layer with thicknesses of 260 and 410 nm were prepared. The films were e-beam deposited onto a Si ⟨100⟩ substrate at room temperature and a thin 15 nm layer of Al, to act as a transducer, was deposited on top of them.

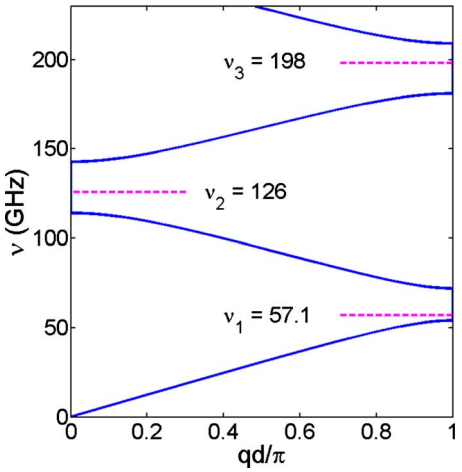

FIG. 1. (Color online) Dispersion of longitudinal acoustic phonons in a Au(5 nm)/Al_2O_3(45 nm) superlattice with first three surface modes marked with a dashed line.

III. THEORY

The multilayer structure under consideration is made up of alternating layers of two different materials of thicknesses d_1 and d_2, densities ρ_1 and ρ_2, and longitudinal sound velocities v_1 and v_2. Since the area excited by the laser pulse is significantly greater then the thickness of the multilayer, only the motion in normal z direction to the surface needs to be considered. Thus, the problem becomes one dimensional and the equation of elasticity is

$$\rho(z)\frac{\partial^2 u(z,t)}{\partial t^2} = \frac{\partial \sigma(z,t)}{\partial z}, \tag{1}$$

where u is the displacement in the z direction, and σ is the zz component of the elastic stress tensor, which is related to u by

$$\sigma(z,t) = \rho v^2 \eta(z,t) = \rho v^2 \frac{\partial u(z,t)}{\partial z}. \tag{2}$$

Here $\eta(=\partial u/\partial z)$ is the zz component of the elastic strain tensor and v is the longitudinal sound velocity. Looking for a solution in the form

$$u(z,t) = u(z)e^{-i\omega t}, \tag{3}$$

and applying the transfer matrix formalism[5,7,8] together with boundary conditions [$u(z)$ and $\sigma(z)$ must be continuous at all interfaces of the superlattice], the dispersion relation can be derived as follows:[10]

$$\cos(qd) = \cos\left(\frac{\omega d_1}{v_1}\right)\cos\left(\frac{\omega d_2}{v_2}\right) - \frac{1}{2}\left(\frac{Z_1}{Z_2} + \frac{Z_2}{Z_1}\right) \times \sin\left(\frac{\omega d_1}{v_1}\right)\sin\left(\frac{\omega d_2}{v_2}\right). \tag{4}$$

Here q is the wave number, $d=d_1+d_2$ is the repeat distance and $Z_i(=\rho_i v_i)$ are the acoustic impedances of the two materials. The calculated dispersion curve for a Au(5 nm)/Al_2O_3(45 nm) superlattice is shown in Fig. 1. For the parameters, we used the bulk values $\rho_2 = 19.3$ g/cm^3, $v_2 = 3.2$ nm/ps, $\rho_1 = 3.97$ g/cm^3, and the experimentally obtained $v_1 = 7.3$ nm/ps. The frequency band gaps where no propagating phonon modes exist are clearly visible.

In case of a semi-infinite superlattice, surface-mode solutions are possible.[7,8] The boundary condition of zero stress at the free surface determines the frequency of the mode, but only when the first layer has a lower acoustic impedance ($Z_1 < Z_2$). This condition holds for all our samples since the first layer is always Al_2O_3. The frequency of a possible surface mode is a solution of[5]

$$p\tan(\omega d_1/v_1) + \tan(\omega d_2/v_2) = 0, \tag{5}$$

where $p = Z_1/Z_2$. The exponential decay length l of the surface mode is given by[1]

$$l = -d/\ln\left|\frac{\cos(\omega d_1/v_1)}{\cos(\omega d_2/v_2)}\right|. \tag{6}$$

The surface mode frequencies calculated using Eq. (5) are marked with dashed horizontal lines in Fig. 1.

Pu (Ref. 4) derived expressions for excitability and detectability of a given normal mode while looking for a solution to Eqs. (1) and (2) in the form $u(z,t) = u_n(z)e^{-i\omega_n t}$:

$$Q_n(t) = -\int \sigma_T(z,t)\,\eta_n(z)dz, \tag{7}$$

$$F_n = \int \eta_n(z) f(z) dz. \tag{8}$$

$Q_n(t)$ represents the optical *excitability* of a normal mode n. It is a spatial overlap integral between the thermal stress σ_T and the strain pattern of the normal mode. Similarly, the optical *detectability* F_n is a spatial overlap integral between the strain pattern η_n and the optical sensitivity function $f(z)$.[1,9] Examples of the optical sensitivity function and the strain patterns of the first two surface modes of a Au(5 nm)/Al_2O_3(45 nm) superlattice are shown in Fig. 2. The photoelastic constants $\partial n/\partial\eta$ and $\partial\kappa/\partial\eta$, where n and κ are the real and imaginary parts of the index of refraction, are needed for calculating the sensitivity function. For Au, we assume $\partial n/\partial\eta = \partial\kappa/\partial\eta$ (Ref. 11) and, using Garfinkel's[12] piezoreflectivity data, we estimate that $\partial n/\partial\eta < 10^{-3}$. This is much smaller when compared to some other metals such as Ni and Cr.[13] However, in the studied multilayers it is also important to know the photoelastic constant of Al_2O_3. Since $\partial n/\partial\eta$ of amorphous Al_2O_3 is not known, we performed a calculation of $\Delta R(t) = \int \eta(z,t) f(z) dz$ while varying the ratio of the photoelastic constants of Au and Al_2O_3. In order to observe the oscillatory signal in the calculated $\Delta R(t)$ similar to the experiment, the photoelastic constant of Al_2O_3 must be smaller than for Au. Figure 2(a) shows the sensitivity function calculated with the ratio $(\partial n/\partial\eta_{\mathrm{Au}})/(\partial n/\partial\eta_{\mathrm{Al_2O_3}}) = 5$. $\Delta R(t) = \int \eta(z,t) f(z) dz$ accounts for the bulk photoelastic effect. However, it was shown by Matsuda *et al.*[14] that in the

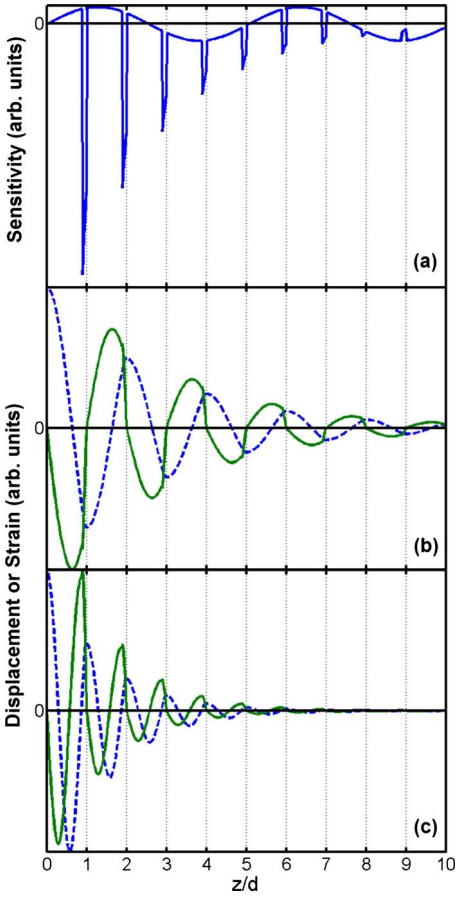

FIG. 2. (Color online) The optical sensitivity function $f(z)$ of Au(5 nm)/Al_2O_3(45 nm) superlattice (a). The strain (full line) and displacement (dashed line) patterns of the first (b) and the second (c) surface mode.

case of semitransparent multilayers, as is our case, the motion of the interfaces can contribute equally to $\Delta R(t)$. Since the photoelastic constants of the superlattices are not known precisely, it is not possible to make a definitive statement about which is the dominant contribution to the observed oscillatory signal, the interface motion or the bulk photoelastic effect.

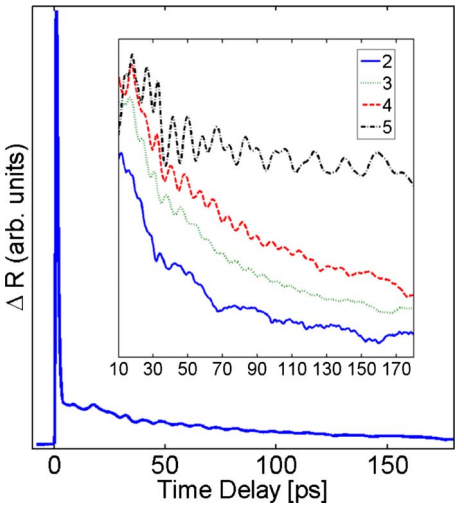

FIG. 3. (Color online) The measured $\Delta R(t)$ for Au(4 nm)/Al_2O_3(45 nm) superlattice. Inset: Zoomed-in oscillatory signal for all Au layer thicknesses. The 5 nm trace was slightly offset for clarity.

IV. RESULTS AND DISCUSSION

A set of regular Au/Al_2O_3 superlattices were studied using time-resolved optical spectroscopy. An example of a measured transient signal $\Delta R(t)$ is shown in Fig. 3. A typical fast transient signal within the first few picoseconds after the arrival of the pump pulse is observed. It is a consequence of the ultrafast excitation of electrons in Au layers and their thermalization through electron-electron interactions, which is then followed by electron-phonon interaction. This leads to heating of the gold layers and generation of thermal stress that initiates surface-mode vibrations. The part of the transient signal starting at 10 ps is zoomed-in in the inset of Fig. 3. All the signals are normalized to the peak value of the fast transient. The trace for the sample with 5 nm Au layers is offset slightly for clarity. The oscillations, which are related to the surface modes, are clearly seen in the traces.

The slow photothermal response superimposed on the oscillatory signals was removed using smoothing and those traces were then analyzed by fast Fourier transform (FFT). The peaks in FFT spectra represent the frequencies of the

TABLE I. Theoretical and experimental surface-mode frequencies of Au(5 nm)/Al_2O_3(45 nm) superlattice. d_{Au} is the gold layer thickness. ν_1 and ν_2 are the frequencies of the first and second surface mode, respectively. l_1 and l_2 are their decay lengths. d is the repeat distance. τ_1 and τ_2 are the decay times of the respective surface modes.

	Theory				Experiment			
d_{Au} (nm)	ν_1 (GHz)	l_1/d	ν_2 (GHz)	l_2/d	ν_1 (GHz)	τ_1 (ps)	ν_2 (GHz)	τ_2 (ps)
2	67.6	9.2	138.7	3.0			166.7	47
3	63.2	5.2	133.0	2.0			128.0	75
4	59.8	3.7	129.0	1.6	59.1[a]	~400	124.7	79.2
5	57.1	2.9	126.0	1.4	53.9	~500	124.2	74.5

[a]Pump at 800nm, probe at 400 nm.

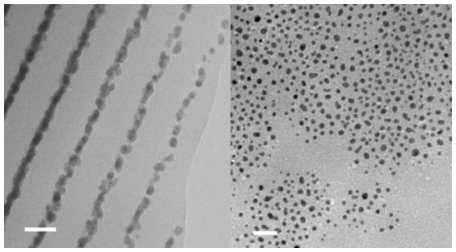

FIG. 4. Cross-sectional (left) and planar (right) TEM images of Au(2 nm)/Al_2O_3(20 nm) multilayer (scale bars=20 nm). The surface is parallel to the Au layers in the cross-sectional image (left).

surface modes. The experimental results compared to the theoretical calculations of Eqs. (4) and (6) are listed in Table I. The first surface mode, which exists in the first zone-boundary ($q=\pi/d$) band gap was detected only in the two samples with the thickest Au layers of 4 and 5 nm. However, the second surface mode, which is in the first zone-center ($q=2\pi/d$) band gap, was observed for all Au layer thicknesses. The highest observed frequency was 166.7 GHz. Any higher frequency modes are not observed, largely due to mode selection rules.[15] Furthermore, the speed of the onset of the thermal stress puts a limit on the highest excited frequency. By fitting the fast transient signals, we obtained an onset time of ~1.2 ps ($\nu<1$ THz), which correlates well with the *e-p* interaction time of Au (~1 ps).[16]

In most of the cases, the experimental frequencies ν_{exp} agree to within a few percent with the theoretical ones ν_{th}. There is, however, a large discrepancy between theory and experiment for the 2 nm Au layer thickness sample. One of the possible causes of this discrepancy is the structure of the gold layer. Figure 4 shows cross-sectional and planar TEM images of a Au(2 nm)/Al_2O_3(20 nm) superlattice that was prepared under same conditions as all our other films. The nanoparticle structure of the Au films is obvious. The size of the nanoparticles ranges up to 5 nm in diameter. This is in contrast with the theory model, which assumes continuous layers with sharp interfaces, so it suggests the nanoparticle structure of the 2 nm Au film as the cause of the discrepancy between experiment and theory. However, it is well known that, under typical deposition conditions, gold does not form a continuous layer until its thickness is over 5 nm.[17] This leads to the conclusion that all our films have nanoparticle structure, in which the particles get closer together and slightly larger as the thickness of the Au film increases, gradually approaching a continuous layer. This assumption is supported by optical spectra shown in Fig. 5. The broad surface plasmon peak can be seen in the spectrum of the 2 nm Au layer superlattice at ~650 nm. It is not only broad but also significantly redshifted due to the interaction among the nanoparticles within each Au layer. The plasmon width and the redshift increase together with increasing Au layer thickness. It seems that even though all the Au films have nanoparticle structure, starting at 3 nm thickness, it does not significantly affect the overall elastic properties of the superlattice as a whole. Looking at Table I, the theoretical frequencies for Au layers >3 nm are slightly larger than the experimental ones. This was observed in several other studies,[3,5,15] which explored the possible origin of the discrepancy in modified elastic properties of thin films, surface modifications of the constituent layers or the accuracy of the layer thicknesses. The nanoparticle structure of our Au films can affect all of these properties.

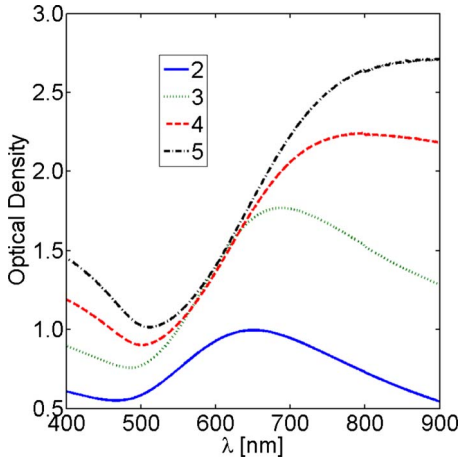

FIG. 5. (Color online) Optical spectra of the superlattices with various Au layer thicknesses.

The exponential decay length defined by Eq. (6) is related to the penetration depth of a particular surface mode into the superlattice. Figures 2(b) and 2(c) show the strain patterns of the first two surface modes of Au(5 nm)/Al_2O_3(45 nm) multilayer. In a study of metallic multilayers,[5] it was suggested that the attenuation rate of the surface mode is inversely proportional to the decay length. While the attenuation rate is also the inverse of the decay time τ, it means that the longer the decay length of a given surface mode is, the longer its decay time should be. In the data on the second surface mode in Table I, no such trend is observed. This implies that the damping of the second surface mode in these samples is not driven by the scattering and absorption of the phonons at the free surface. The damping is likely dominated by scattering at the nanoparticle Au films. Since data for the first surface mode are available only for two samples, it is not possible to make a similar conclusion about the causes of its damping, but it can be seen that the first surface mode decays more slowly then the second one. This is mainly due to the lower frequency of the first surface mode, which is equivalent to longer wavelengths and therefore less scattering.

There are several possible reasons why the first surface mode is only observed in the 4 and 5 nm Au layer thick samples. The decay lengths of the first mode shown in Table I are increasing with decreasing Au layer thickness, which means that the modes are extending deeper into the superlattice. However, our multilayers have only 10 periods, which might not be enough for the first surface mode in the 2 and 3 nm Au layer thick samples. Further, we used the Eqs. (7) and (8) to evaluate the optical excitability and detectability of the surface modes. The finite element analysis (COMSOL) was used to model the multilayer structure. The heating of the Au layers in the model was chosen so that it corresponds to the experimental conditions such as light absorption in each Au layer and the thermal stress onset time of 1 ps. The obtained thermal stress $\sigma_T(z,t)$ was then used to numerically calculate

TABLE II. Excitability and detectability of the surface modes. Excitability is time dependent function, so only its maximum from within first 50 ps window is presented. For comparison, all values are normalized to the values of Au(5 nm)/Al_2O_3(45 nm) superlattice.

d_{Au} (nm)	$Q_{1_M}/Q_{1_{M5}}$	$Q_{2_M}/Q_{2_{M5}}$	F_1/F_{1_5}	F_2/F_{2_5}
2	0.21	0.35	0.25	0.68
3	0.43	0.58	0.43	0.76
4	0.75	0.78	0.73	0.87
5	1	1	1	1

$Q_n(t)$. $Q_n(t)$ is a time-dependent function, but the time evolution of this function is very similar for all samples, so for comparison we just assumed its maximum value Q_{n_M} within the modeled time range. The values of Q_{n_M} normalized to the values of 5 nm Au layers $Q_{n_{M5}}$ for the first and second surface modes are shown in Table II. As the Au layer thickness decreases, the maximum of the optical excitability decreases more rapidly for the first surface mode. The ratio of the excitability between the surface modes favors the second one, $Q_2/Q_1 \approx 6$. The trend seen in the optical excitability is also observed in the optical detectability. Overall, the optical excitability and detectability are also compelling reasons for the observation of the first surface mode only in the 4 and 5 nm Au layer thick samples.

The surface modes that lie in the phononic band gap are not the only modes that can be excited and detected in the superlattice structure. The normal modes with real q can be excited simultaneously with them as well. In a perfect multilayer with sharp interfaces, these normal modes are Bloch waves. They propagate freely without any scattering or reflections at the interfaces. In the case of a semi-infinite superlattice, the normal modes propagate into the film and are not detected since they leave the detection sensitive surface region. However, in the case of finite superlattices the normal modes can get reflected from the substrate interface and return to the surface where they can be detected. We observe such modes in our Au(5 nm)/Al_2O_3(45 nm) sample. Figure 6 shows the background-subtracted signal past the fast transient peak. The signal was fitted using a least-squares fitting routine and was successfully decomposed into an exponentially decaying cosine function representing the first surface mode and the two echoes that represent the propagating normal modes arriving at the surface after being reflected at the substrate interface. The Fourier transform is used to analyze the frequency components of the measured signal (Fig. 7). The sharp peak of the first surface mode and the broader peak of the second surface mode can be easily identified in Fig. 7. The broad peak at lower frequencies below the first surface mode represents the propagating normal modes that consist of the modes on the lowest minibranch of the zone-folded longitudinal phonon dispersion curve shown in Fig. 1. The Fourier transform of the echo signal alone, shown in Fig. 7 as a dashed curve, confirms that the broad peak consists of these normal modes.

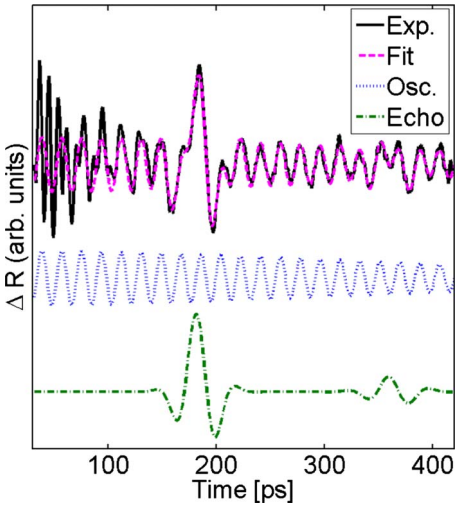

FIG. 6. (Color online) Zoomed-in oscillatory trace with thermal signal subtracted of Au(5 nm)/Al_2O_3(45 nm) superlattice and its fit. Fitted curve, obtained using least-squares fitting, is decomposed into its exponentially decaying cosine function (Osci.—dotted curve) and the two echoes (Echo—dot-dashed curve).

The main cause of the decreasing amplitude of the echoes is the reflection at the Al_2O_3/SiO_2 interface. The acoustic reflection coefficient r is defined by[18]

$$r = \frac{Z_2 - Z_1}{Z_2 + Z_1}, \tag{9}$$

where $Z_{1,2}$ are the acoustic impedances. Using these values for the density and velocity of sound for fused silica $\rho_{SiO_2} = 2.2\ \mathrm{g/cm^3}$ and $v_{SiO_2} = 5.97\ \mathrm{nm/ps}$,[19] the calculated reflection coefficient is −0.38. The minus sign means there is a π phase shift during the reflection. The ratio of the amplitudes of the second echo to the first one is only 0.2, which suggests there is another damping mechanism that attenuates the

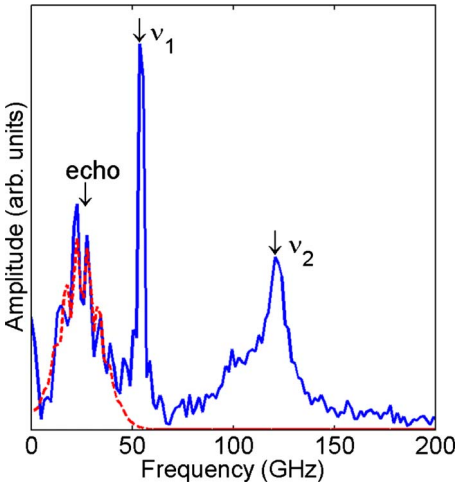

FIG. 7. (Color online) The Fourier transform spectra of the background subtracted signal of the Au(5 nm)/Al_2O_3(45 nm) superlattice shown in Fig. 6. The dashed curve represents the Fourier transform of the echo signal only.

stress pulse as it propagates in the superlattice. The most likely cause of this attenuation is the phonon scattering at the Au layers.

The normal modes travel through the superlattice at an effective sound velocity given by[20]

$$v_{\text{eff}} = \frac{d}{\sqrt{\frac{d_1^2}{v_1^2} + \frac{d_2^2}{v_2^2} + \left(\frac{Z_1}{Z_2} + \frac{Z_2}{Z_1}\right)\frac{d_1 d_2}{v_1 v_2}}}. \quad (10)$$

The evaluation of this expression for our Au(5 nm)/Al_2O_3(45 nm) superlattice yields 6.2 nm/ps. It is possible to compare this to an experimental value obtained from the ratio $2l/t$, where l is the thickness of the whole superlattice and t is the time difference between the two echoes. The thickness of the superlattice, measured by profilometry, is $l=540\pm20$ nm. The echoes are separated by $t=179.4\pm4$ ps. That leads to the effective sound velocity of 6 ± 0.3 nm/ps. Within the margin of error, this is in agreement with the theoretical prediction.

V. SUMMARY

We have used time-resolved pump-probe technique to study the surface acoustic modes of four Au/Al_2O_3 multilayers with different Au layer thicknesses (2 to 5 nm) and low relative metal thickness ratio Γ. The second surface mode was observed in all samples, but the first surface mode was observed only in the samples with the thicker 4 and 5 nm Au layers. The frequency of these modes was compared to the theory calculation and good agreement was generally found. The slight differences are not attributed to the softening of the effective longitudinal elastic constant, but to the effect of the nanoparticle structure of the Au films. The analytical expressions for the detectability and excitability were evaluated and provide an insight into the reasons why the first surface mode is observed only in the samples with thicker Au layers. In addition to the surface modes, the normal phonon modes were observed in the Au(5 nm)/Al_2O_3(45 nm) superlattice. They belong to the lowest minibranch of the zone-folded longitudinal phonon dispersion curve and travel in the form of a propagating pulse, which is reflected at the substrate and surface interfaces. Detecting two echoes of the pulse makes it possible to experimentally determine the effective sound velocity in the superlattice.

The present results show that the multilayer theoretical analysis works well even for structures with large differences in constituent layer thicknesses. This conclusion supports the usefulness of the theoretical modeling of superlattices in designing structures with predefined positions of the surface mode frequency peaks.

ACKNOWLEDGMENTS

We would like to thank X. X. Liang for doing the TEM analysis and F. Lenz for preparation of the single Al_2O_3 layer films. This work was supported in part by the National Science Foundation GOALI program (grant No. DMR-0513048), the Office of Science U.S. Department of Energy (grant No. DE-FG02-01ER45916), and the McMinn Endowment at Vanderbilt University.

*Also at Materials Science and Technology Division, Oak Ridge National Laboratory, Oak Ridge, TN 37831, USA.

[1] H. T. Grahn, H. J. Maris, J. Tauc, and B. Abeles, Phys. Rev. B **38**, 6066 (1988).
[2] A. Yamamoto, T. Mishina, Y. Masumoto, and M. Nakayama, Phys. Rev. Lett. **73**, 740 (1994).
[3] C. Rossignol, B. Perrin, B. Bonello, P. Djemia, P. Moch, and H. Hurdequint, Phys. Rev. B **70**, 094102 (2004).
[4] N.-W. Pu, Phys. Rev. B **72**, 115428 (2005).
[5] W. Chen, Y. Lu, H. J. Maris, and G. Xiao, Phys. Rev. B **50**, 14506 (1994).
[6] B. M. Clemens and G. L. Eesley, Phys. Rev. Lett. **61**, 2356 (1988).
[7] R. E. Camley, B. Djafari-Rouhani, L. Dobrzynski, and A. A. Maradudin, Phys. Rev. B **27**, 7318 (1983).
[8] B. Djafari-Rouhani, L. Dobrzynski, O. Hardouin Duparc, R. E. Camley, and A. A. Maradudin, Phys. Rev. B **28**, 1711 (1983).
[9] C. Thomsen, H. T. Grahn, H. J. Maris, and J. Tauc, Phys. Rev. B **34**, 4129 (1986).
[10] S. M. Rytov, Akust. Zh. **2**, 71 (1956) [Sov. Phys. Acoust. **2**, 68 (1956)].
[11] O. B. Wright, Phys. Rev. B **49**, 9985 (1994).
[12] M. Garfinkel, J. J. Tiemann, and W. E. Engeler, Phys. Rev. **148**, 695 (1966).
[13] T. Saito, O. Matsuda, and O. B. Wright, Phys. Rev. B **67**, 205421 (2003).
[14] O. Matsuda and O. B. Wright, J. Opt. Soc. Am. B **19**, 3028 (2002).
[15] N.-W. Pu and J. Bokor, Phys. Rev. Lett. **91**, 076101 (2003).
[16] O. B. Wright and V. E. Gusev, Physica B **219-220**, 770 (1996).
[17] L. Zhang, R. Persaud, and T. E. Madey, Phys. Rev. B **56**, 10549 (1997).
[18] L. E. Kinsler, A. R. Frey, A. B. Coppens, and J. V. Sanders, *Fundamentals of Acoustics* (John Wiley & Sons, New York, 1981).
[19] R. Vacher and J. Pelous, Phys. Rev. B **14**, 823 (1976).
[20] B. Bonello, B. Perrin, E. Romatet, and J. C. Jeannet, Ultrasonics **35**, 223 (1997).